

The relationship between undularity and l dependence of the proton optical model potential

R. S. Mackintosh*

School of Physical Sciences, The Open University, Milton Keynes, MK7 6AA, UK

(Dated: February 15, 2019)

Abstract

The contribution of collective or reaction channels to a local optical model potential, OMP, can be readily calculated as a dynamical polarization potential, DPP. The resulting local DPPs commonly have undulatory ('wavy') features, often including local regions of emissivity in the imaginary component. We show here that this undularity arises from l -dependence of the underlying formal non-local and l -dependent DPP. The l -independent proton OMPs, that have the same S -matrix S_{lj} as phenomenological l -dependent potentials, exhibit undulations that are qualitatively similar to undulations of local DPPs generated by channel coupling. The l -dependent phenomenological potentials studied are the potentials that give the best existing fits to the relevant elastic scattering data and the undulatory potentials presented here, being S -matrix equivalent (i.e. having the same S -matrix, S_{lj}) give exactly the same scattering. In addition, we present calculations strongly suggesting that undularity ('waviness') is a generic property of l -independent potentials that are S -matrix equivalent to l -dependent potentials. Implications for the validity of folding models based on a local density model are noted.

PACS numbers: 25.40.Cm, 24.50.+g, 24.10.Ht, 03.65.Pm

*Electronic address: raymond.mackintosh@open.ac.uk

I. INTRODUCTION

Following the proposal [1] that the nucleon optical model potential (OMP) is explicitly l -dependent, it was often suggested that an l -independent potential with a suitably modified radial form would fit the data equally well. That turns out to be true, but the undulatory (wavy) radial forms that are required to fit precise and wide angular range data were not anticipated. Three lines of investigation converge regarding the radial form of the nucleon OMP: (i) experimental elastic scattering observables that could not be precisely fitted with smooth Woods-Saxon (WS), or similar, forms can be fitted precisely with potentials exhibiting undulations, (ii) the local and l -independent dynamic polarisation potentials (DPPs) generated by coupling to reaction or inelastic channels are significantly undulatory, often with emissive regions, (iii) an l -dependent potential model exists that gives fits over a wide energy range to data that cannot be fitted with WS-like potentials. References supporting points (i), (ii) and (iii) are given in what follows. Arguments that it is a worthwhile enterprise to get precise fits to highly accurate, wide angular range elastic scattering data are presented in Ref. [2]. Arguments that the possibility of angular momentum dependence should be kept open, and a general review of angular momentum dependence of nuclear potentials, will be found in Ref. [3].

Which of the alternative forms of potential, undulatory or l -dependent, is more natural? This is relevant to the application of OMPs in reaction analyses since two S -matrix equivalent potentials will generally not lead to the same radial wave function in the nuclear interior. In this work, ‘ S -matrix equivalent potentials’ are potentials with the same S -matrix S_{lj} where l and j are the partial-wave orbital and total angular momenta for spin $\frac{1}{2}$ projectiles. Such potentials clearly give exactly the same observables, so fits to elastic scattering alone can not lead to a preference for l -dependent or undulatory potentials. Here we attempt to establish a correspondence between l -dependence and undularity. The key point is that for any l -dependent potential, we can determine an S -matrix equivalent l -independent potential.

Undularity not only occurs in precision fits to high quality elastic scattering data: the local and l -independent representations of the dynamical polarisation potentials, DPPs, generated by coupling to transfer or inelastic channels are generally undulatory. Such DPPs commonly have radial regions where the imaginary part is emissive. For nucleon scattering examples, see e.g. Refs. [4–8]. Although emissive regions in DPPs may appear surprising,

the nature of their origin ensures that the unitarity limit $|S_{lj}| \leq 1$ is not broken.

It is natural to ask how the undularity of DPPs can be interpreted, and how it can be linked to fits of scattering data. Regarding the link to data, we will show that a phenomenological l -dependent potential model, successfully applied to the elastic scattering of 30 MeV protons from ^{16}O , ^{40}Ca , ^{58}Ni and ^{208}Pb , has undulatory l -independent equivalents at each energy, the imaginary terms often having emissive regions. These potentials have features that are similar to features appearing in local DPPs resulting from inelastic-channel or reaction-channel coupling, Refs. [4–8].

In this work we apply S -matrix inversion to determine the l -independent potentials that are S -matrix equivalent to l -dependent proton potentials that fit elastic scattering data. The resulting S -matrix equivalent l -independent potentials have qualitative features, namely undularity and regions of emissivity, that are also found in local and l -independent DPPs arising from channel coupling. Such l -independent DPPs are thus the equivalents of l -dependent potentials. This is reasonable since l -dependence is a property of the formal DPPs, as in the theory of Feshbach [9], see also Rawitscher [10]. As mentioned above, potentials with undulatory features are found when fitting light-ion elastic scattering data that is both precise and having a wide angular range, see Section VII. The occurrence of undulations, and the lack of any widely understood interpretation of them, may inhibit the exact fitting of such data. Data of that quality arguably contain information concerning the dynamics of nucleon-nucleus and nucleus-nucleus interactions [2].

Every l -dependent potential has an l -independent equivalent which can be found using $S_{lj} \rightarrow V(r) + \mathbf{I} \cdot \mathbf{s} V_{\text{SO}}(r)$ inversion, see Section II. Section III presents systematic properties of the l -independent potentials that have the same S_{lj} as l -dependent potentials precisely fitting proton scattering. Section IV discusses issues arising. Section V presents the radial properties of the inverted potentials. The l -dependent potentials in earlier sections give precise fits to elastic scattering data, but in Section VI S -matrices for potentials having simpler forms of l dependence are inverted in order to assess whether undularity, including emissivity, is a generic property of potentials that are S -matrix equivalent to l -dependent potentials. Section VII discusses direct model-independent fits to elastic scattering. Section VIII relates l -dependence to nuclear size. Section IX is a summary and Section X is an appendix specifying the characteristics of the l -dependent potentials.

II. *S*-MATRIX INVERSION

The *S*-matrices are inverted using the iterative-perturbative, IP, $S_{lj} \rightarrow V(r) + \mathbf{l} \cdot \mathbf{s} V_{\text{SO}}(r)$ inversion algorithm which is presented in Refs. [11–14]. The IP inversion is implemented in the inversion code IMAGO [15] which quantifies the difference between the S_{lj}^t to be inverted and the S_{lj}^i of the inverted potential in terms of the *S*-matrix distance σ defined as

$$\sigma^2 = \sum_{lj} |S_{lj}^t - S_{lj}^i|^2. \quad (1)$$

The IP iterations start from a ‘starting reference potential’, SRP, which in all cases presented here was the *l*-independent part of the *l*-dependent potential. The plots of the inverted potentials presented here are produced by IMAGO and include the SRP. The contribution of the *l*-dependence to the inverted *l*-independent potential thus appears as the difference between the inverted potential and the SRP. It has been established that the IP method can yield inverted potentials that are effectively independent of the SRP and the uniqueness of the inverted potential can be tested by the use of alternative ‘inversion bases’, see Refs. [12, 14]. The figures produced by IMAGO include the values of σ and in cases where two inverted potentials are shown, that with the lower σ is generally adopted. The tendency for undularity to increase as σ becomes very small will be addressed in relation to the significance of the potential undulations.

III. *l*-INDEPENDENT EQUIVALENT OF *l*-DEPENDENT PHENOMENOLOGY

The *S*-matrix elements S_{lj} , (SMEs), have been inverted for the following *l*-dependent potentials: 30.1 MeV protons on ^{16}O and 30.3 MeV protons on ^{40}Ca from Ref. [16], and for 30.3 MeV protons on ^{58}Ni and ^{208}Pb from Ref. [17]. These *l*-dependent potentials fitted the data with a precision exceeding that achieved with other potentials, and vary more smoothly with energy than the best *l*-independent fits. The ^{16}O and ^{40}Ca cases are notoriously hard to fit, and cannot be fitted with non-undulatory forms. The inverted potentials having the same S_{lj} as the *l*-dependent potentials obviously reproduce the data equally well.

The *l*-dependent potentials [16, 17] all consist of standard-form *l*-independent potentials to which *l*-dependent real and imaginary surface peaked terms are added, see the Appendix. We invert S_{lj} for the *l*-dependent potential to obtain the *l*-independent equivalent; subtracting from this the *l*-independent part of the *l*-dependent potential gives an *l*-independent

measure of the l -dependent effect. Rather than plot all the resulting difference potentials, we quantify the l -dependence in terms of volume integrals as defined by Satchler [18]. We present the differences between the volume integrals of the l -independent equivalent potentials and the l -independent part of the l -dependent potential. The differences in the volume integrals of the real and imaginary central terms are ΔJ_R , ΔJ_{IM} with similar notation for the spin-orbit (SO) terms. These are presented in Table I for three cases: (i) when only the imaginary l -dependent terms is included, (ii) when only the real l -dependent terms is included and, (iii) when both l -dependent terms are included, as required to fit the data. The significance of the additivity of the real and imaginary l dependencies will be addressed in forthcoming work.

The four main sections of Table I are headed by an identification of the case, e.g. 30.1 MeV protons on ^{16}O , etc. The first column labels what is presented on the line: four sets of changes in volume integrals and one set of changes in the reaction cross section, CS. The remaining four columns present the differences between volume integrals for (i) the S-matrix equivalent l -independent potential found for various l -dependent potentials, and, (ii) the same volume integrals for the l -independent potential to which the l -dependent parts had been added. Column 2 presents the effect of the full l dependence, column 3 is for imaginary l dependence alone, column 4 is for real l dependence alone. The last column simply adds numbers in columns 3 and 4 for comparison with the corresponding numbers in column 2, reflecting on the linearity of the system to the inclusion of real and/or imaginary l -dependent terms. We note:

1. For the ^{16}O case, in column 4, the real l dependence alone resulted (no surprise) in a large change in ΔJ_R and a smaller change in ΔJ_I . The large change in ΔJ_R is associated with a very small change in the reaction cross section (CS) but simultaneously a very large change in angular distribution (AD) beyond 80° , and in the analysing power (AP) for all angles, see Fig. 1.
2. Also for ^{16}O , as expected, the imaginary l dependence gave a somewhat larger volume integral change ΔJ_I than ΔJ_R ; for real l dependence the change ΔJ_R was much greater than the change in ΔJ_I . (In this case, the imaginary l -dependent term was at a much larger radius than the real l -dependent term [16].) As expected, the change in CS is very large for the imaginary l -dependent term, Fig. 2. The changes in the AD and

TABLE I: Properties of potentials that are l -independent equivalents to l -dependent phenomenological potentials. For each quantity, the same quantity for the l -independent part of the l -dependent potential has been subtracted, leaving differences ΔJ_R and ΔJ_I etc.. All volume integrals are in terms of MeV fm³ and the change in reaction cross section, CS, due to the inclusion of the l -dependent terms, Δ CS is in mb. The last column presents the numerical sum of the values in columns 3 and 4.

	Full-Ldep	IM-Ldep	RE-Ldep	Σ RE+IM
p + ¹⁶ O 30.1 MeV				
ΔJ_R	-27.25	6.55	-37.21	-30.66
ΔJ_I	9.4	11.43	0.09	11.52
ΔJ_{SOR}	0.612	0.626	0.289	0.915
ΔJ_{SOI}	0.46	0.671	0.011	0.682
Δ CS	55.41	52.25	0.37	52.62
p + ⁴⁰ Ca 30.3 MeV				
ΔJ_R	-69.21	2.09	-71.59	-69.50
ΔJ_I	13.649	6.439	7.059	13.498
ΔJ_{SOR}	1.4124	0.0213	1.4874	1.5087
ΔJ_{SOI}	-0.1451	-0.0991	-0.09098	-0.1901
Δ CS	53.13	38.81	20.66	59.47
p + ⁵⁸ Ni 30.3 MeV				
ΔJ_R	-38.85	0.09	-40.93	-40.84
ΔJ_I	8.346	0.995	6.463	7.458
ΔJ_{SOR}	1.1533	-0.0501	1.3573	1.3072
ΔJ_{SOI}	-0.1263	-0.0526	-0.1578	-0.2104
Δ CS	29.3	6.2	23.8	30.0
p + ²⁰⁸ Pb 30.3 MeV				
ΔJ_R	-6.82	0.04	-6.59	-6.78
ΔJ_I	1.98	0.46	1.88	2.34
ΔJ_{SOR}	0.1009	-0.0056	0.1061	0.1005
ΔJ_{SOI}	0.4891	0.3829	0.0636	0.4465
Δ CS	10.1	8.3	2.3	10.6

AP are less than for real l -dependence, Fig. 1, except at angles forward of 80° . This might also be related to the large radius of imaginary l -dependent term.

3. The values in the last (Σ) column are quite close to those in the ‘Full’ column. Exact additivity cannot be expected.
4. Points 1 and 2 together exemplify the strong disconnect between the magnitudes of the changes in CS and the changes in the angular observables. This is relevant to evaluating the contribution of fitting the CS when determining OMP parameters.
5. Similar general results apply for ^{40}Ca , ^{58}Ni and ^{208}Pb targets, but with diminishing importance of the imaginary l -dependence for the heavier targets.
6. In spite of point 5, and the diminishing effect of l -dependence for the heavier targets, the general properties of the l -dependence are basically the same for all four target nuclei. This goes back to the claim of Refs. [16, 17] that the general properties of the l -dependent potential, that ‘precisely’ fits all the data, vary with energy much more regularly than the best l -independent WS-type fits (which fit the data poorly).

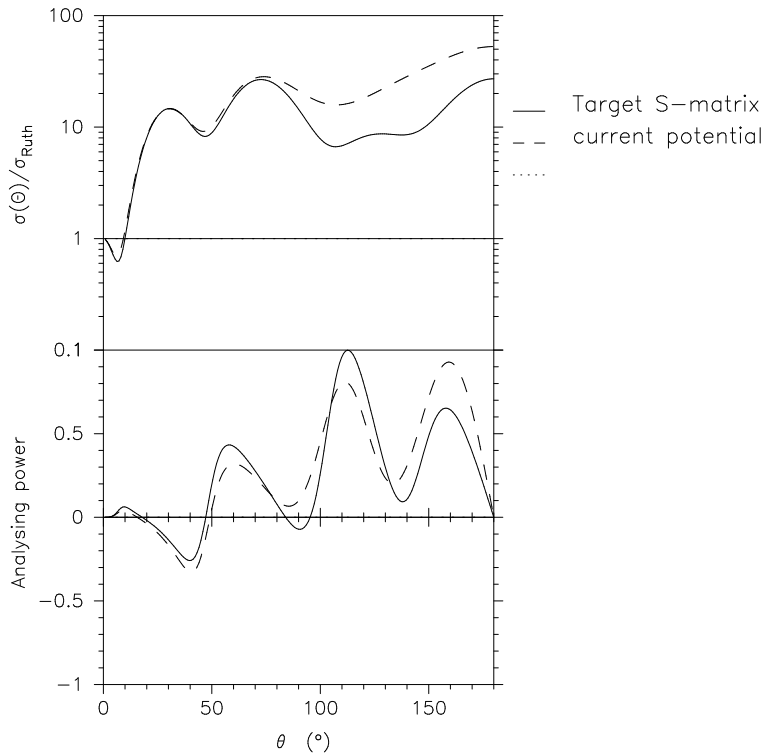
In Section V, we show that the l -independent S -matrix equivalents to l -dependent potentials that actually fit proton elastic scattering have undulations (waviness) in the surface, including regions of emissivity. Since the l -dependent potentials are the only potentials that currently fit all the relevant proton elastic scattering data, it follows that the only l -independent potentials that currently fit those data have emissive regions in the surface (and undularities not just in the surface.) This is significant since the dynamic polarisation potentials Refs. [4–8] arising from various channel couplings exhibit such undularities.

A. Higher energy ^{40}Ca case

The l -dependent potential in Ref. [16] for 35.8 MeV protons on ^{40}Ca had a somewhat different character from the 30.3 MeV potential since the l -independent imaginary part was predominantly of volume character whereas that for 30.3 MeV had surface absorption. This case could therefore help answer the question: how does the character of the inverted l -independent potentials depend on the form of the l -independent part of the l -dependent potential? The 35.8 MeV case was studied without spin-orbit terms.

FIG. 1: For 30.1 MeV protons on ^{16}O , the solid lines are the angular distribution (above) and analyzing power (below) with just the real l -dependence included. The dashed lines are calculated with the same potential but with the l -dependent terms omitted. The associated change in reaction cross-section was very small: just 0.37 mb.

IMAGO cross-sections - 173703.784 on 20170114

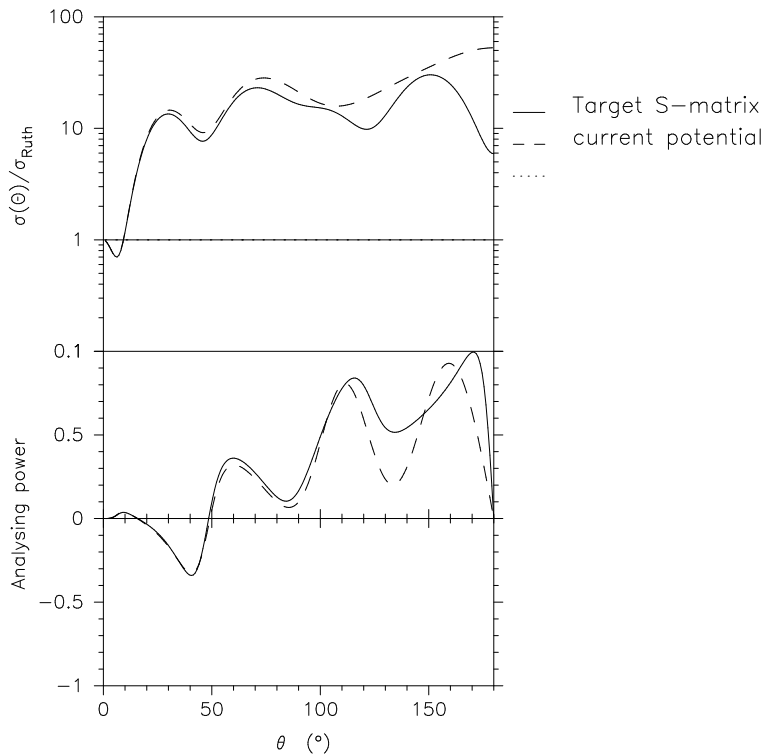


The form of the l -dependent term was like that for 30.3 MeV. Characteristics of the resulting inverted l -independent potentials are presented in Table II, in the format of Table I, for full l -dependence as well as for separate real and imaginary l -dependence. In Section V, the resulting inverted real potential will be seen to have a form very similar to that for 30.3 MeV, the imaginary term had very similar undulations (including emissivity) in the surface but with some differences in the nuclear interior. When the real and imaginary terms were added separately, it was found that real l dependence led to a real part that is visually the same as for full l dependence. However, real l -dependence led to only a very small amplitude undularity in the imaginary potential in the surface, $r > 6$ fm, region, although there was some effect for $r < 6$ fm.

With l -dependence of just the imaginary part, there was little effect on the real potential,

FIG. 2: For 30.1 MeV protons on ^{16}O , the solid lines are the angular distribution (above) and analyzing power (below) with just the imaginary l -dependence included. The dashed lines are calculated with the same potential but with the l -dependent terms omitted. The associated change in reaction cross-section was 52.25 mb.

IMAGO cross-sections - 103145.779 on 20170119



but the imaginary potential had a form that was hard to distinguish, except for $r < 5$ fm, from that with full l dependence. By eye, the effect of the full l dependence was just the sum of the effects of real and imaginary l -dependent components. This is in accord with what is shown in the last column of Table II.

IV. PROPERTIES AND QUERIES ARISING

Tables I and II reveal various systematic effects directly related to the properties of the l dependence that was required to fit the data. The following properties merit interpretation:

P1 The real l -dependence in all cases is such as to reduce the attraction for the lowest

TABLE II: Properties of potentials that are l -independent equivalent to l -dependent 35.8 MeV phenomenological potentials for protons on ^{40}Ca . For each quantity, the same quantity for the l -independent part of the l -dependent potential has been subtracted, leaving differences ΔJ_{R} and ΔJ_{I} . All volume integrals are in MeV fm^3 and the change in reaction cross section, ΔCS , due to the inclusion of the l -dependent terms, is in mb. The last column has the sum of the values in columns 3 and 4.

	Full-Ldep	IM-Ldep	RE-Ldep	Σ RE+IM
$\text{p} + ^{40}\text{Ca} \text{ 35.8 MeV}$				
ΔJ_{R}	-69.75	1.90	-72.08	-70.18
ΔJ_{I}	13.74	9.51	2.90	12.41
ΔCS	10.67	8.88	1.67	10.55

partial waves. (Hence negative ΔJ_{R} in all RE-Ldep cases)

P2 The imaginary l -dependence in all cases acts to increase the absorption for lowest partial waves (hence positive ΔCS and positive ΔJ_{I} in all IM-Ldep cases).

Note that both these properties are consequences of the l -dependent components of the overall l -dependent potentials, and are not related to any comparison with the best (i.e. least worst) l -independent potential [16, 17] .

Two questions arise:

Q1 Why does l -dependence in the *real* part always act to increase J_{I} (positive ΔJ_{I})?

Possible answer: from **P1**, the lowest partial waves are subject to less attraction and hence the local wave number is reduced allowing greater absorption along the trajectory. Effectively, the nucleon slows down somewhat and spends more time in the absorptive region. This can easily be seen in terms of the complex momentum of the nucleon within the complex potential. (There will also be refractive effects.)

Q2 Why does the *imaginary* l -dependence tend to increase J_{R} ?

Possible answer: As expected from **P2**, the real potential becomes somewhat less effective for small radii where partial waves with low l are most sensitive. But, the effect must not apply for partial waves with large l so the reduced attraction at the centre is compensated by a region of attraction near the surface which leads to an increase in volume integral. The

attractive region near 5 fm connects to undulations in the far surface. Hence the intuition that there should be repulsion is fulfilled for small r , but the r^2 weighting of the volume integrals wins out, leading to positive ΔJ_R .

The tentative nature of the answers suggests that there is much still to be learned about the simplest aspects of nuclear elastic scattering.

V. RADIAL FORM OF THE INVERTED POTENTIALS

Tables I and II present magnitudes of various properties of the l -dependent contribution to the l -independent equivalent potential. Here we show explicitly the undularity and emissiveness induced in the l -independent equivalent potentials. The inverted potentials for the ^{16}O , ^{40}Ca and ^{58}Ni 30 MeV cases are presented in Fig. 3 to Fig. 5 respectively, and for 35.8 MeV protons on ^{40}Ca in Fig. 6. In these figures the solid lines represent the l -independent part of the l -dependent potential and the dashed or dotted lines represent l -independent potentials having the same S_{lj} as the l -dependent potential. Thus ΔJ_R etc. in Table I relate to the differences between the solid and dashed or dotted lines.

Two inverted potentials are presented for ^{16}O and ^{40}Ca , the lower values of σ corresponding to extended iterations of the IP inversion. For ^{58}Ni there was just one series of iterations and the dashed line, coincident in this case with the solid line, represents both the l -independent part of the l -dependent potential and the SRP; here σ has fallen in the inversion process from an initial value of 0.926 for the SRP to 0.134×10^{-3} .

The vertical scales of the various components in Fig. 3 to Fig. 6 have been adjusted to the magnitude of each quantity plotted. Noting this, the amplitude of the undularity in the far surface of the real central potential is comparable to that of the imaginary potential. Apart from the ^{16}O case, the imaginary spin-orbit term (absent from the l -dependent potential) is very small, and subject to some uncertainty in the inversion process. The large effect on the real, central term is qualitatively the same for each target nucleus: a strong reduction in depth for smaller radii with a transition to an increase in depth near the surface, leading to undulations further out. The imaginary central potential also exhibits qualitative similarities in all cases, including marked surface undularities which clearly include regions of emissivity.

For 35.8 MeV protons on ^{40}Ca , Fig. 6 shows that the modifications of the potential due to the l dependence are qualitatively the same as for 30.3 MeV case; the change from surface to

volume absorption in the l -independent part has made little qualitative difference, especially in the surface region.

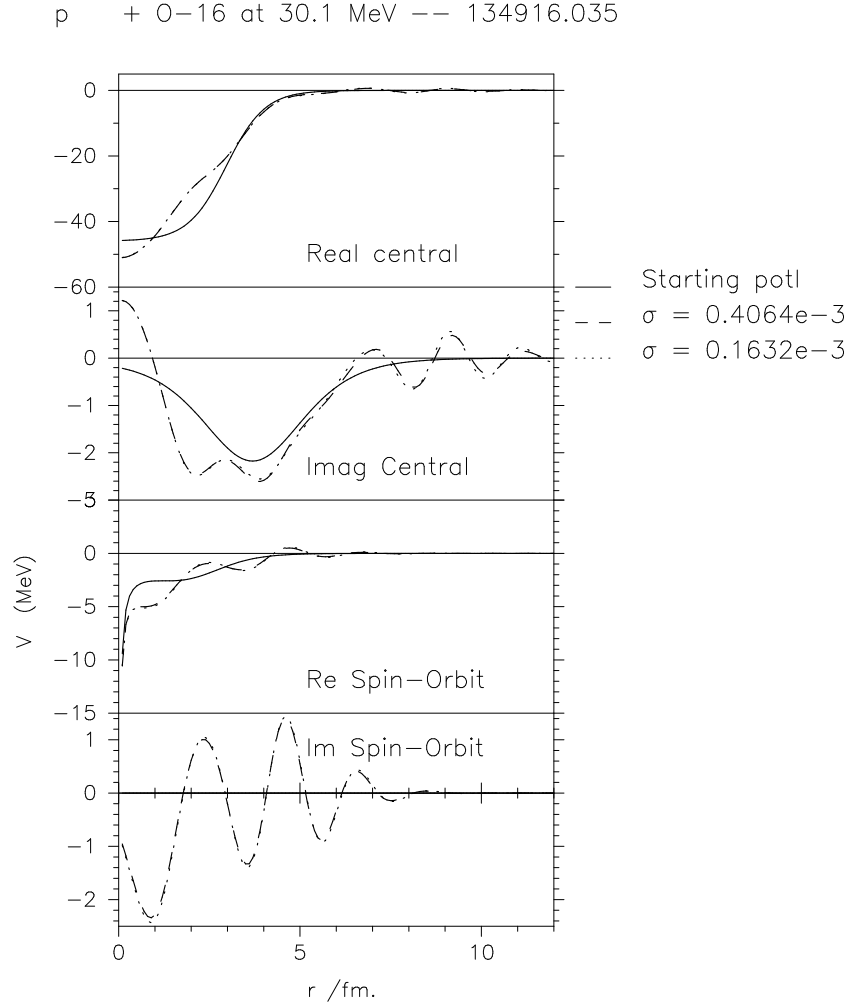
Fig. 3 to Fig. 5, and also Fig. 6, all exhibit a great reduction in the real potential in the nuclear interior while the change in the surface region is actually somewhat attractive. This leads to an increase of rms radius of the inverted real central: for the 30.3 Mev ^{40}Ca case the rms radius of the real part is increased by 0.1568 fm. In the same case, the rms radius of the imaginary central potential is decreased by 0.2112 fm. These are quite large changes, but are intelligible in terms of the properties **P1** and **P2** above.

VI. MODEL CALCULATIONS AND GENERIC PROPERTIES

It is legitimate to ask whether undularity is a generic property of l -independent potentials that are S -matrix equivalent to potentials that are substantially l -dependent. For example, is the occurrence of emissivity in the surface a consequence of the particular surface peaked l -dependent terms of Refs. [16, 17]? It is not easy to give a comprehensive answer to such questions but here the issue is explored with simple model calculations involving an l -dependent potential of WS form. These reveal that a form of l dependence which does not involve a surface peaked l -dependent term also leads to l -independent equivalents that are strongly undulatory in the surface, including emissive regions in the surface of the imaginary term, even when only the real term is l -dependent. Thus the undulations in Section V are not an artefact of the surface peaked nature of the l -dependent component.

There are many ways in which a potential can be l -dependent. Here we study just one in which we apply a uniform renormalisation of the real or imaginary term for low- l partial waves. The transition has the same dependence on L and Δ as that for the previous calculations and specified in the Appendix. The real or imaginary part is multiplied by some factor for l values less than L (chosen as specified below), and not modified for high l , with a transition region defined by Δ . This is motivated by the possibility that l dependence is characterised by a difference between the interaction for partial waves that have a strong overlap with the nucleus and those that do not. At each energy, the value of L is chosen to be the value of l for which $|S_l|$ is close to 0.5. Two values of the transition parameter Δ are chosen to determine whether the amplitudes of the undulations are related to the sharpness of the transition. Here, the spin-orbit terms are omitted. Similar model calculations were

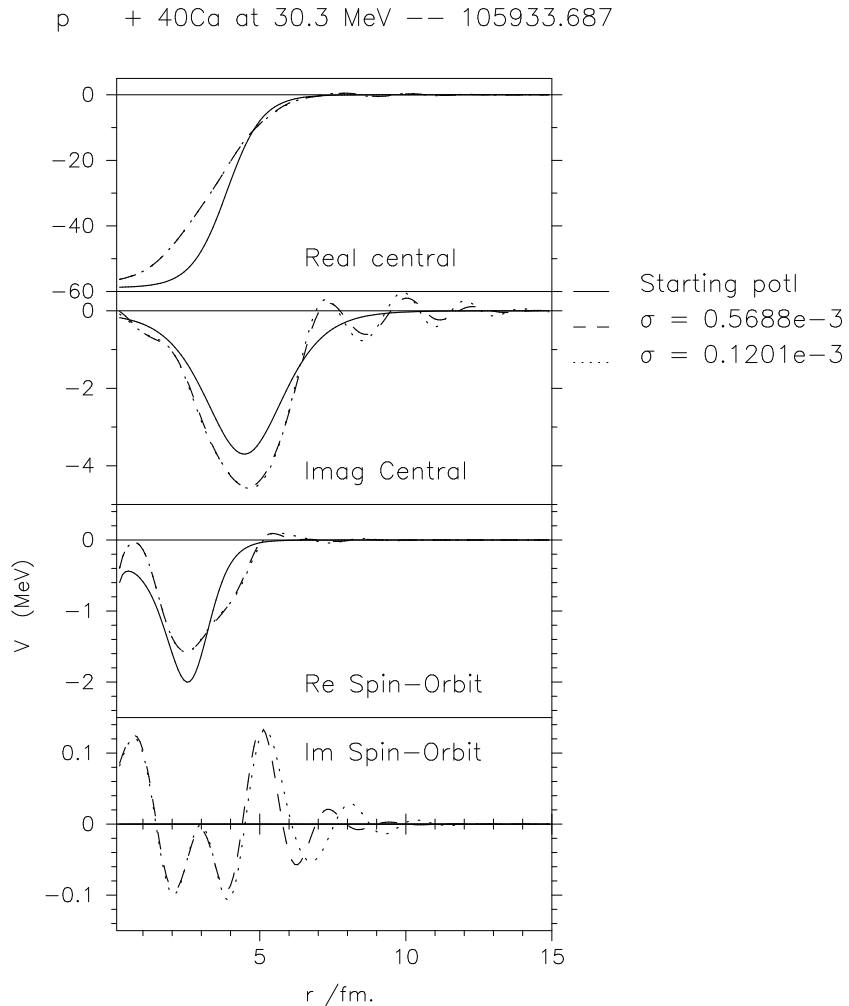
FIG. 3: For 30.1 MeV protons on ^{16}O , the solid lines present the l -independent part of the l -dependent potential. The dashed and dotted lines are the inverted potentials, that with dots having lower inversion σ and is the one with properties given in Table I. From top panel downwards, the real-central, imaginary-central, real spin-orbit and imaginary spin-orbit (the last is zero for the l -independent term.)



carried out, with a similar purpose, in a study [20] of the angular momentum dependence generated by channel coupling in the case of ^{16}O scattering from ^{12}C at 115.9 MeV.

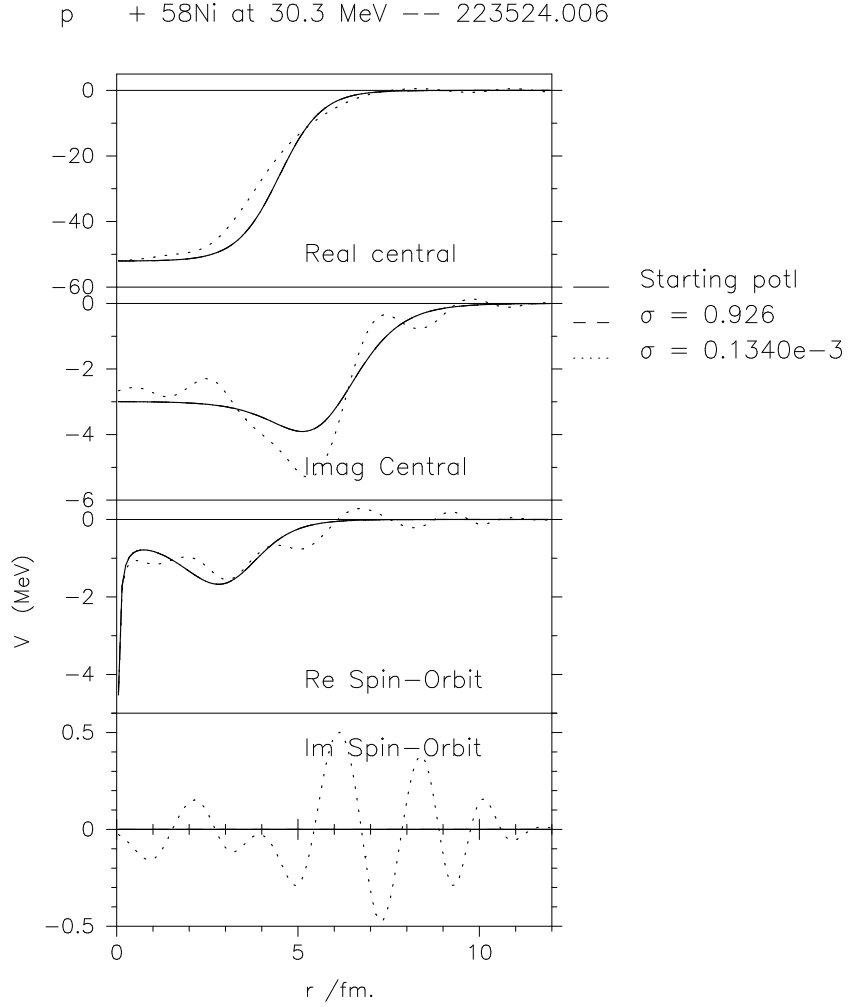
Calculations were performed for 30 MeV and 45 MeV protons scattering from ^{40}Ca . The Koning-Delaroche [26] (KD) potential was used, without the spin-orbit term. For low partial waves, i.e. for l less than L , the real part was reduced by 10 % and was left unmodified for high l . The transition between high and low l was quantified by parameter Δ . Two values,

FIG. 4: For 30.3 MeV protons on ^{40}Ca , the solid lines present the l -independent part of the l -dependent potential. The dashed and dotted lines are the inverted potentials, that with dots having lower inversion σ and is the one with properties given in Table I. From top panel downwards, the real-central, imaginary-central, real spin-orbit and imaginary spin-orbit (the last is zero for the l -independent term). The radial scale is different from that of Fig. 3.



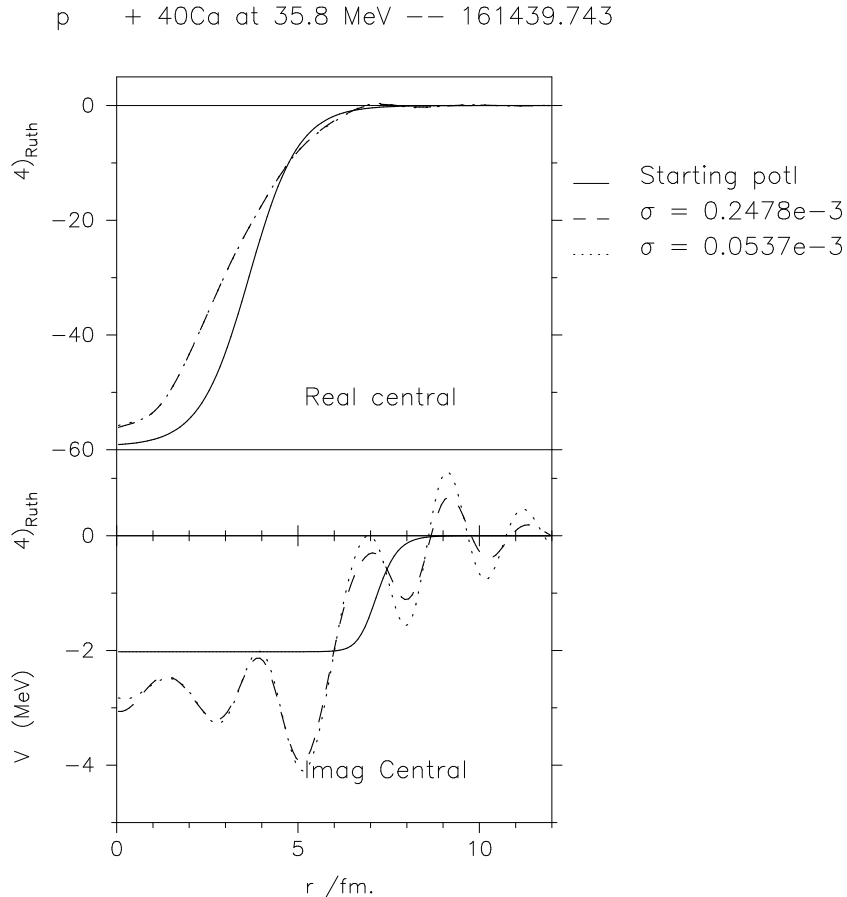
$\Delta = 1$ and $\Delta = 2$, were used at 30 MeV to verify that a smaller Δ leads to stronger undulations. For 30 MeV we set $L = 5.5$ and for 40 MeV we set $L = 6.5$. The volume integrals of the real and imaginary potentials J_R and J_I for the inverted l -independent potentials are calculated and the corresponding volume integrals for the KD potential are subtracted. The differences, ΔJ_R and ΔJ_I , giving a measure of the l -independent representation of the effect of the l -dependence, are presented in Table III. The percentage changes are also pre-

FIG. 5: For 30.3 MeV protons on ^{58}Ni , the solid lines present the l -independent part of the l -dependent potential. The dotted lines are for the inverted potentials, with properties given in Table I. The dashed lines follow the solid lines, and the very large initial inversion sigma, 0.926, is given. From top panel downwards, the real-central, imaginary-central, real spin-orbit and imaginary spin-orbit (the last is zero for the l -independent term).



sented, as are changes in the reaction cross section, ΔCS . Consistent with the l -dependent modification being confined to the real part, ΔCS is very small although the change in the angular distribution is quite large. These changes are consistent with a uniform decrease in the real phase shift, for $l < L$. There were also changes in $|S_l|$, both positive and negative for different l , leading to a small change in CS of about 0.5 mb at 30 MeV and only about 0.2 mb at 45 MeV. However, at 45 MeV, the differential cross section was reduced at all

FIG. 6: For 35.8 MeV protons on ^{40}Ca , the solid lines present the l -independent part of the l -dependent potential. The dotted lines are for the inverted potential with the lowest inversion σ and the properties given in Table II. Top panel: the real-central; lower panel: imaginary-central.



angles except near 150° where it was quite small.

These results are presented twice in Table III for the 30 MeV cases and three times for the 45 MeV case, corresponding to different values of the S -matrix distance σ defined in Eq. 1. The multiple solutions at each energy bring out a point that is relevant for evaluating the surface undulations. As the iterations for the $S_l \rightarrow V(r)$ inversion proceed, the undulations in the potential become more pronounced and this is related to the values of σ given in Table III. The discussion below refers to potential identifiers, P.I. (pot1 etc.).

The angular distributions for the l -independent (inverted) potentials closely fitted that from the l -dependent potentials, for 45 MeV, see Fig. 7. The lower value of σ corresponds to a small improvement to the fit to the angular distribution, but corresponds to a substantial

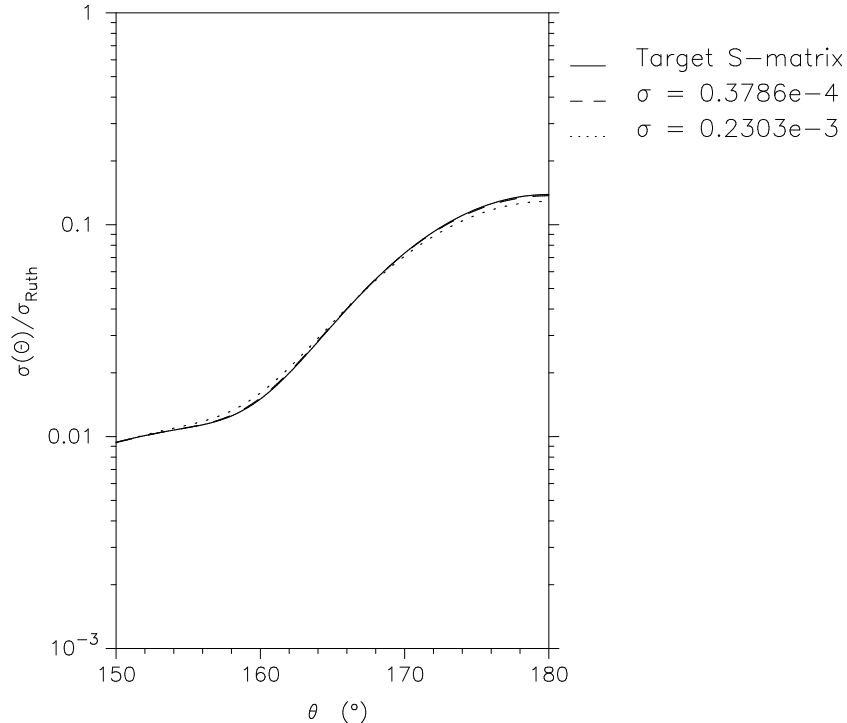
improvement in the reproduction of S_l for l values that make very little contribution to the angular distribution. Specifically the improvements in fits to S_l were for $l > 11$ at 30 MeV and $l > 14$ at 45 MeV. In the latter case, $|S_{14}| \sim 0.9997$ and $\arg S_{14} \sim 10^{-4}$ and the change in the angular distribution corresponding to the correction of S_l by further iterations was $< 10\%$ at 180° .

TABLE III: Properties of potentials that are l -independent equivalents to l -dependent phenomenological potentials. The differences in the real and imaginary volume integrals, ΔJ_R and ΔJ_I , and the same changes expressed as percentages, are given. All volume integrals are in MeV fm^3 and the change in reaction cross section, CS, due to the inclusion of the l -dependent terms, ΔCS is in mb. The percentage change is also given. P.I. is the potential identifier.

Energy	L	Δ	P. I.	σ	ΔJ_R	$\Delta J_R \%$	ΔJ_I	$\Delta J_I \%$	ΔCS	$\Delta \text{CS} \%$
Real part l -dependent										
30.0	5.5	1	pot2	1.66×10^{-4}	-39.47	-9.56	5.09	4.44	0.52	0.399
30.0	5.5	1	pot1	1.88×10^{-5}	-41.12	-9.96	10.37	9.04	0.52	0.399
30.0	5.5	2	pot1	4.13×10^{-5}	-35.67	-8.64	3.41	2.97	0.55	0.420
30.0	5.5	2	pot2	3.55×10^{-6}	-35.82	-8.69	3.92	3.42	0.55	0.420
45.0	6.5	2	pot1	2.30×10^{-4}	-32.15	-8.77	1.59	1.44	0.207	0.208
45.0	6.5	2	pot3	3.79×10^{-5}	-32.67	-8.91	2.96	2.70	0.206	0.207
45.0	6.5	2	pot4	4.02×10^{-5}	-32.52	-8.87	2.43	2.22	0.206	0.207
Imaginary part l -dependent										
30.0	5.5	2	pot1	1.41×10^{-5}	1.76	0.426	8.59	7.49	3.33	2.55
30.0	5.5	2	pot2	5.64×10^{-6}	1.78	0.431	8.58	7.48	3.33	2.55

The three 45 MeV cases show how improving the fit to S_l for high l , thereby lowering σ , increases the undularity but with only small improvements to the angular distribution. We illustrate this with the pot3 which was the end point of a different sequence of inversion iterations. Fig. 7 shows that the angular distribution for pot1 differs from that calculated with the l -dependent potential by 10 % at most near 180° , while the dashed line, representing pot3, is almost indistinguishable from the solid line. The potentials pot1 and pot3 are compared with the l -independent part of the l -dependent potential in Fig. 8.

FIG. 7: For 45 MeV protons on ^{40}Ca , The solid line represents the angular distribution between 150° and 180° calculated with the l -dependent potential. The dashed line, virtually indistinguishable from the solid line, is calculated with the l -independent potential pot3, with inversion $\sigma = 3.79 \times 10^{-5}$. The dotted line corresponds to an earlier iteration, pot1, with $\sigma = 2.30 \times 10^{-4}$.

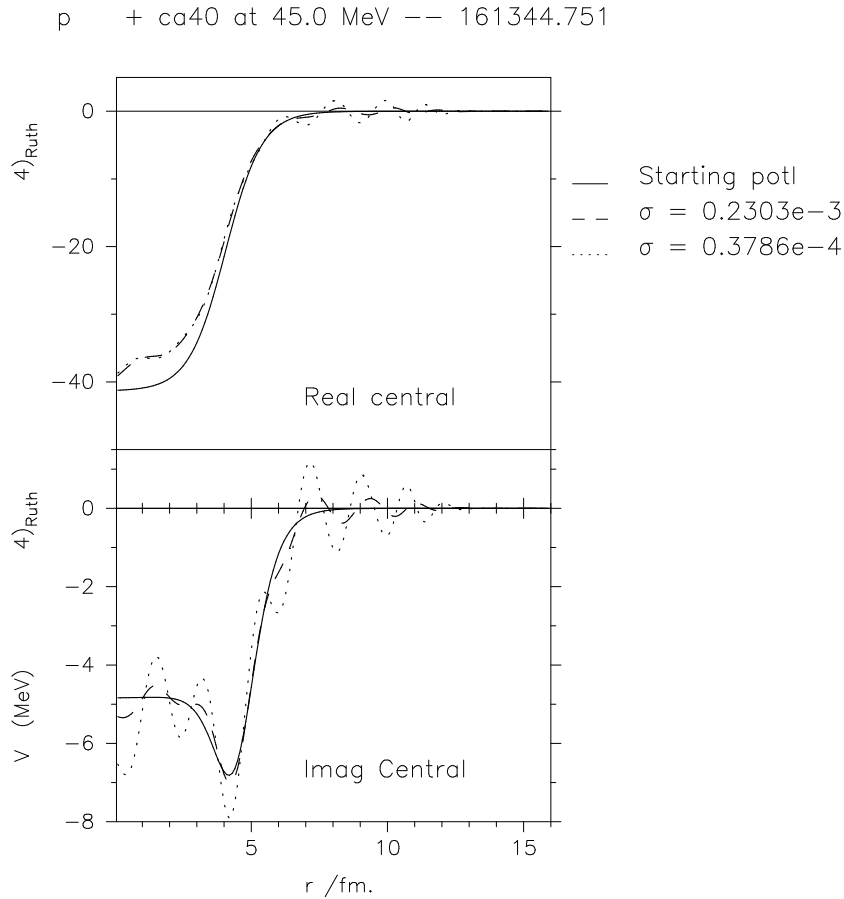


The higher value of σ for pot1 is due to the poor fit to S_l for high values of l , as presented in Fig. 9. It is apparent that to reproduce S_l for $l > 14$ simultaneously with reproducing S_l for low l , larger amplitude undulations are required. Thus an exact representation, with an l -independent potential, of S_l from an l -dependent potential of the present form, requires undulations having an effect on the angular distribution beyond present experimental capabilities.

A. l dependence of the imaginary component

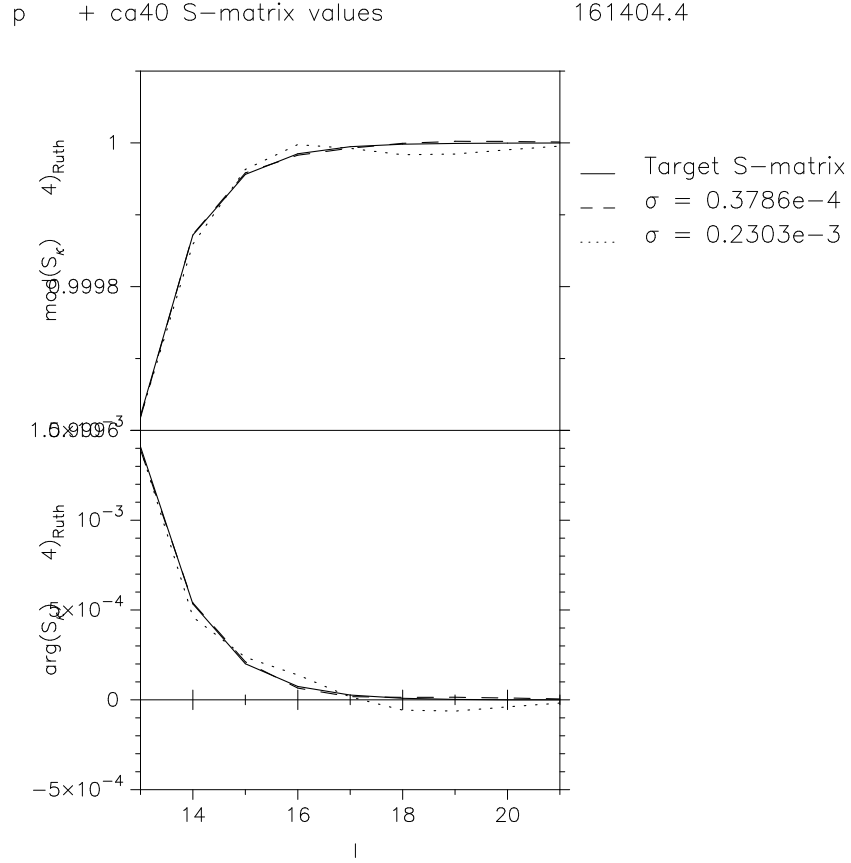
To examine the effect of l dependence in the imaginary potential, the imaginary potential for 30.0 MeV is increased by 10 % for low partial waves, with $L = 5.5$ and $\Delta = 2$. Inverting was straightforward for this relatively small perturbation yielding potentials having low values of σ and characteristics given in the lowest two lines of Table III.

FIG. 8: For 45 MeV protons on ^{40}Ca , the solid lines present the l -independent part of the l -dependent potential with the real part in the top panel and the imaginary part below. The dashed lines represent the inverted potential for the 45 MeV pot1 of Table III and the dotted lines are for the inverted potential pot3 of that table. The potential pot4 of that table is very close to pot3.



Unsurprisingly the l -dependent increase of the imaginary potential led to a much greater increase in the reaction CS than with the stronger real l -dependence. The increase in J_I of somewhat less than 10 % is unsurprising, as is the small percentage change in J_R . A uniform l -independent 10 % increase in the imaginary potential would, of course, lead to J_I increasing by 10 % with zero change in J_R , and no undulations. There is little change to the real part in the interior region. The undulations resulting from the l -dependent increase can be seen in Fig. 12 which also shows that there is an increase in the imaginary potential of roughly 10 % for r up to about 4.5 fm. For larger radii the imaginary potential oscillates about an average of roughly zero change. At around 9 fm, these undulations include an

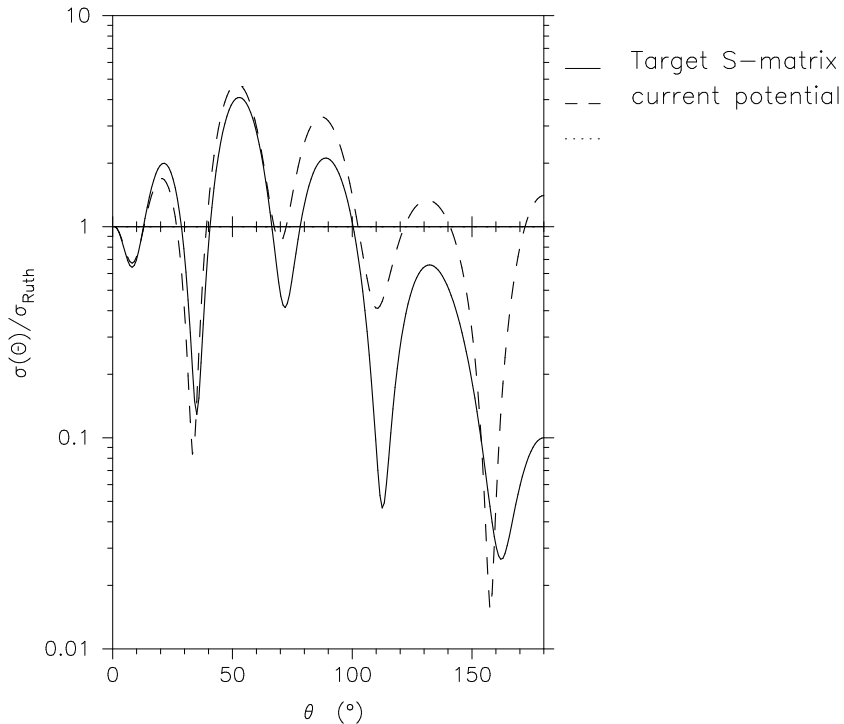
FIG. 9: For 45 MeV protons on ^{40}Ca , the upper panel presents $|S_l|$ and the lower panel $\arg S_l$ for three cases. The solid line is calculated directly from the l -dependent potential, the dotted lines are S_l calculated with l -independent potential pot1 and the dashed lines, hard to distinguish from the solid lines, present S_l calculated with pot3.



emissive region. This is clearer in the expanded scale of Fig. 13 which also shows that there are undulations in the real part that have a similar amplitude to the undulations in the imaginary part. It is a common feature in these studies to find that surface undulations in either the real or the imaginary part are accompanied by undulations in the other. The potential pot2 improves the fit to $|S_l|$ for between $l = 12$ and $l = 18$; $|S_l| \simeq 0.99992$ for $l = 12$, but makes no visible change to the elastic scattering angular distribution. It appears that the undulations in the surface are driven by the requirement to fit the highest partial waves with a single potential for all partial waves.

The real and imaginary l -dependencies have contrasting effects on the reaction cross sections and the elastic scattering angular distributions. From Table III it can be seen that

FIG. 10: For 30 MeV protons on ^{40}Ca , the dashed line represents the angular distribution without any l -dependency and the solid line represents the angular distribution for the case of the real l dependence (10 % increase) with $L = 5.5$ and $\Delta = 2$.

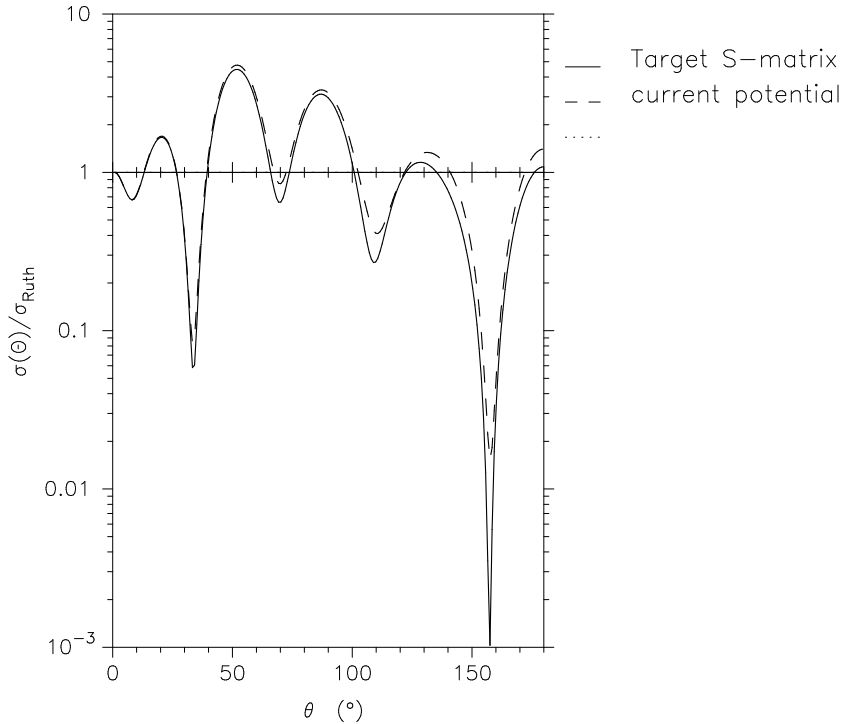


the real l -dependent term has quite a small effect on the reaction cross section, CS, (about 0.42 % at 30 MeV with $\Delta = 2$) whereas the imaginary l dependence increased CS by 2.5 %. By contrast, the real l dependence had a large effect on the elastic scattering angular distribution, see Fig. 10, whereas the imaginary l dependence had a much smaller effect on the angular distribution, as in Fig. 11. This is an example of the large disconnect between changes in elastic scattering angular distributions and changes in reaction cross sections.

VII. l -INDEPENDENT FITS TO ELASTIC SCATTERING DATA

Fitting precise, wide angular range, elastic scattering data with an l -independent potential leads to a potential having strong undulations. This was shown for protons on ^{16}O and ^{40}Ca , see Ref. [21]. The fits to data in this reference were intended to be unprejudiced by theory and were almost model independent. ‘Almost’ model independent because a constraint was imposed to ensure that the imaginary term was not emissive at any radius. This was

FIG. 11: For 30 MeV protons on ^{40}Ca , the dashed line represents the angular distribution without any l -dependency and the solid line represents the angular distribution for the case of the imaginary l dependence defined in the text..

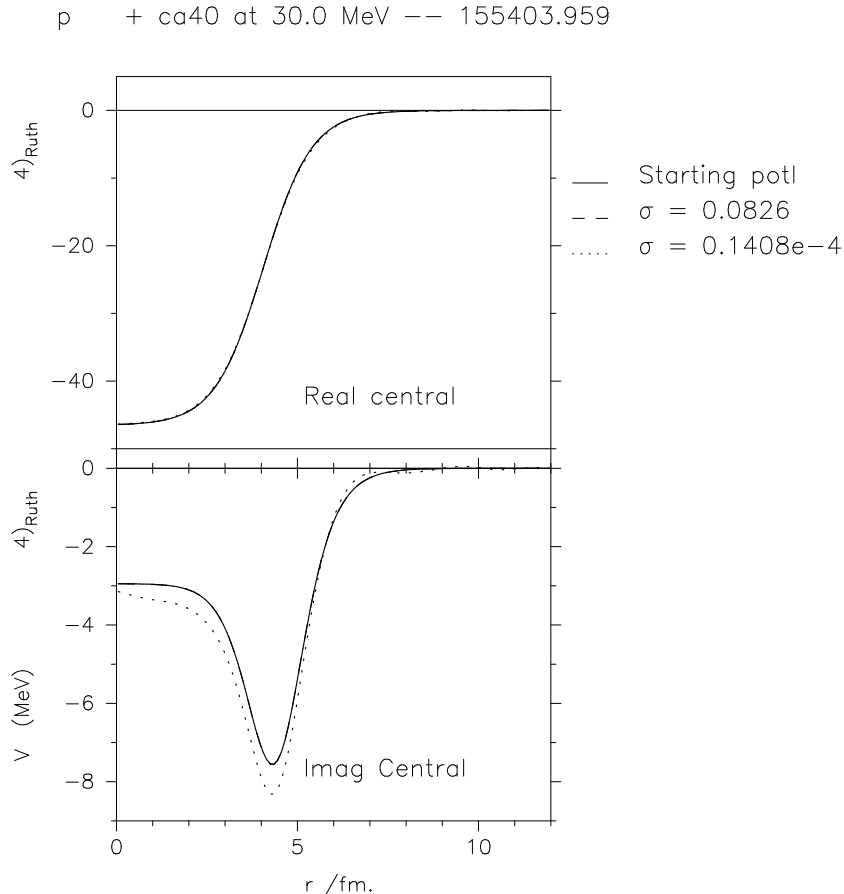


actually a theoretical prejudice and the present work shows that this constraint is a mistake. However, the general finding that strong undulations are required for an l -independent fit stands, although the form of the undulations are distorted by what is now evidently an improper constraint.

Such undulations are not confined to potentials fitting proton elastic scattering. For deuteron scattering see Refs. [22, 23] and for heavier projectiles see, for example, Refs. [24, 25]. We conclude that, to achieve low χ^2 fits to precise and wide angular range elastic scattering data, the possibility of undularity must not be excluded.

The undulations referenced in this section have an amplitude far exceeding variations in the radial density of the target nuclei. The potential undulations are therefore not a direct reflection of undulations in the nuclear density and it is hard to imagine any explanation other than S -matrix equivalence to l -dependent potentials.

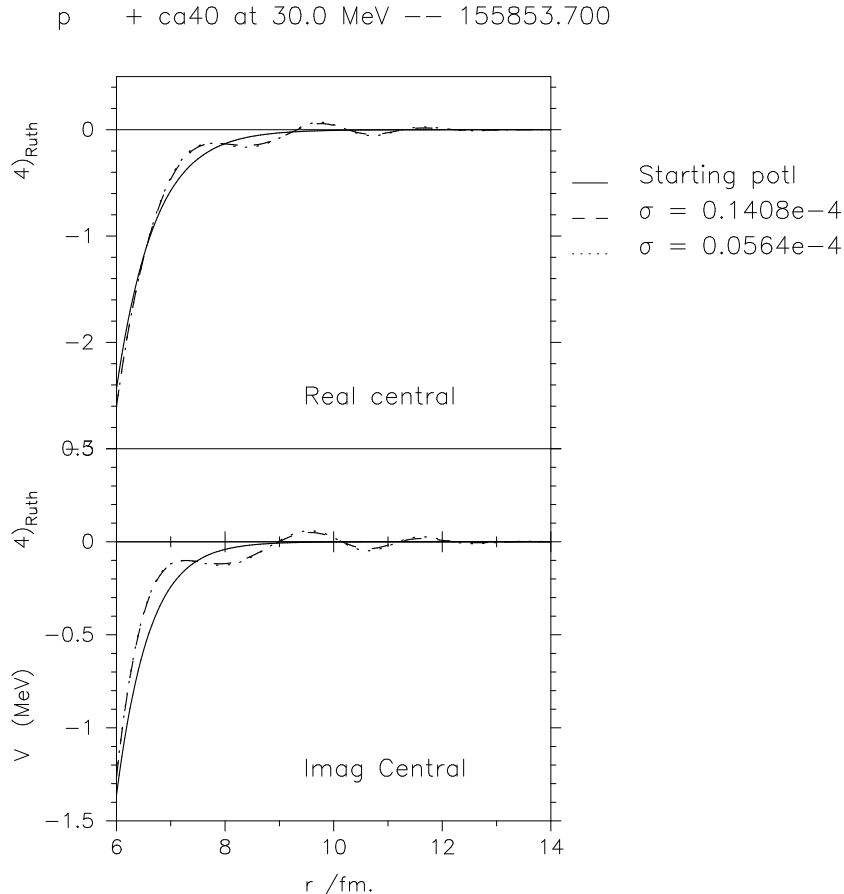
FIG. 12: For 30 MeV protons on ^{40}Ca , the solid lines and hidden dashed lines present the l -independent part of the l -dependent potential with the real part in the top panel and the imaginary part below. The dotted lines represent the inverted potential for the 30 MeV pot1 in the lowest part of of Table III. The potential pot2 of that table is indistinguishable from pot1 out to at least 12 fm.



VIII. THE RELATIONSHIP OF l -DEPENDENCE TO NUCLEAR MASS

Table I suggests that the empirically fitted l -dependence becomes less important as the nuclear mass increases. Most calculations of OMPs assume a local density model which does not explicitly take into account consequences of the density gradient in the nuclear surface. The l dependence can be seen as a consequence of reaction processes occurring in the presence of gradients in the nuclear density. It is then of interest to quantify the comparative importance of the surface region where nuclear density gradients are substantial and examine the relationship between this and the degree of l -dependence for nuclei of

FIG. 13: For 30 MeV protons on ^{40}Ca , the solid lines represent the l -independent part of the l -dependent potential with the real part in the top panel and the imaginary part below. The dotted lines and dashed lines represent, respectively, the inverted potentials pot1 and pot2 in the lowest part of Table III. The potential pot2 of that table is indistinguishable from pot1 out to at least 12 fm.



different masses. We have therefore calculated the ratio R_S of the volume integral of the nucleon OMP calculated in two ways:

$$R_S = \int_0^{\mathcal{R}} V(r)r^2 dr \left[\int_0^{\infty} V(r)r^2 dr \right]^{-1} \quad (2)$$

In the first integral, the upper limit $\mathcal{R} = (R - a)$ where R is the radius parameter of the Woods-Saxon potential and a is the WS diffusivity. Therefore, R_S is a measure of the volume fraction of the OMP that is interior to the surface region, in particular the region where the potential has a substantial radial gradient.

We have calculated R_S for ^{16}O , ^{40}Ca , ^{58}Ni and ^{208}Pb . In each case, we calculated R_S for

the real central term of the Koning Delaroche global potential [26]. The values for those four nuclei, were, respectively: 0.254, 0.426, 0.466, 0.642. All of these numbers point to the importance of the surface region, but most particularly ^{16}O stands out as being in a separate class. If l -dependence is, as we propose, related to the influence of surface processes, and strongly influenced by departures from the validity of local density approximation, then we should not be surprised to find strong effects associated with l -dependence for ^{16}O . It would be interesting to know what part of the effect due to channel coupling, e.g. to deuteron channels [27], is accounted for in local density folding models.

IX. SUMMARY AND DISCUSSION

Section III presented characteristic properties of l -independent potentials that were found by inversion to be S -matrix equivalents of l -dependent potentials. The particular l -dependent potentials give excellent fits to elastic scattering data that cannot be fitted with conventional radial forms. Section V compared the inverted potentials with the l -independent part of each l -dependent potential and Figs. 3 to 5 show that each l -independent potential found by inversion has undulations in the surface. The undulations in the imaginary terms include radial regions where the potential is emissive. This tendency is strongest for light target nuclei and persists to a smaller degree for the ^{208}Pb case, not shown. Since the S_{lj} for l -dependent potentials all satisfy the unitarity bound, this is true also for the inverted potentials, despite the emissive regions. It follows that l -independent potentials that fit elastic scattering of 30 MeV protons from ^{16}O , ^{40}Ca , ^{58}Ni and ^{208}Pb , probably better than any other potentials, have undularities with emissive regions in the nuclear surface. Since they are the l -independent equivalents of l -dependent potentials, it is reasonable to attribute undularity and emissivity found in phenomenological potentials to an underlying l dependence. It is also reasonable to attribute the appearance of undularity and emissivity in local DPPs from coupled channel calculations, determined by inversion of S_l or S_{lj} , to the l dependence of an underlying non-local and l -dependent DPP.

Does the strong undularity, involving emissive regions, result from the particular form of l dependence applied in Refs. [16, 17]? That particular l -dependent term was quite sharply confined to the surface region. The calculations presented in Section VI suggest that the occurrence of undularity is a generic property of potentials that are l -independent S -matrix

equivalents of l -dependent potentials. In that section the l -independent equivalents were found for potentials for which the real or imaginary part was multiplied by a factor over a range of partial waves: $l < L$ with a transition over a range $\sim \Delta$. For the real part, the factor was 0.9 and for the imaginary part, 1.1. The resulting potentials were undulatory. The undulations in the l -independent potential had regions of emissivity in the imaginary part as a result of l dependence in either the real or imaginary terms. The sharpness of the l -dependence transition was adjustable, and a sharper transition (smaller Δ) led to somewhat stronger undulations. A similar relationship between l -dependence and undularity was found in the case of ^3He scattering on ^{58}Ni [28] and also found for ^{16}O scattering from ^{12}C at 115.9 MeV [20]. *It therefore appears that there is a generic relationship between undulations in optical potentials and an underlying l dependence.*

In Section VIII we presented a plausible argument for the l -dependence of proton OMPs becoming weaker as the mass of the target nucleus increases, as suggested by the results in Table I.

Implications: Any necessity for l dependence indicates a failure of a folding model based on a local density approximation. Thus, for any case of elastic scattering, if a precise model-independent, but l -independent, empirical fit to wide angular range precise data exhibits undulations, then the actual potential for that case must be l -dependent, indicating a failure of local density folding models. In this situation, it is unclear what potential is appropriate for use in direct reactions. This must depend on what channels are included and the use of local l -independent potentials is unjustified. Since DPPs never amount to a uniform renormalization, it is clear also that the appropriate way to evaluate a folding model potential is by fitting a model-independent additive term, when data of suitable quality exists.

The key point is that imprecise fits to nuclear elastic scattering data of typical range and precision miss key physics; there appear to be historical reasons why precision fitting of nuclear scattering data is not taken as seriously as precision fitting of electron scattering data. A possible disincentive for treating l -dependence is the uncertainty as to how to incorporate the consequences of causality, i.e. dispersion relations that must hold between the real and imaginary potentials. This has been studied for a particular form of l -dependence in Ref. [29].

X. APPENDIX: SPECIFICATION OF THE l -DEPENDENCE

The l dependence adopted in Refs. [16, 17] and of Section III was essentially that of the original work, Ref. [1]. The l -dependent potential was the sum of a standard l -independent term with an added l -dependent term. The l -independent term was a Woods-Saxon real part plus an imaginary part that was the sum of Woods-Saxon and Woods-Saxon derivative terms. A conventional spin-orbit term was included and all terms were as defined by Perey and Perey [19]. The l dependency of was in the form of an additional central potential having real and imaginary Wood-Saxon derivative (surface peaked) form with an overall l -dependent factor:

$$f(l) = \frac{1}{1 + \exp((l^2 - L^2)/\Delta^2)}. \quad (3)$$

Thus, the l -dependence has the form of an additional surface potential that cuts off sharply when $l > L$. There is the one overall l -dependent factor $f(l)$ for both real and imaginary parts which had independent radial and strength parameters. There was no l -dependence in the spin-orbit term which was real in almost all cases. This l -dependent potential fitted the data with very consistent parameters, the values of which varied more smoothly with energy than the parameters of the best l -independent potentials. In all cases, the searches led to a real l -dependent term that was repulsive (i.e. there was less attraction for $l \ll L$) and an imaginary term that was absorptive (i.e. more absorption for $l \ll L$.) This is immediately reflected in the volume integral results in Table I.

Potentials for Section VI. The real l -dependence of Section VI was achieved by adding a repulsive real potential of identical form to the original real potential but of one tenth the magnitude and with overall factor $f(l)$ of Eq. 3. Thus the potential is reduced by 10 % for low partial waves. The imaginary l dependence was effected in a similar fashion.

-
- [1] R.S. Mackintosh, and L.A. Cordero, Phys. Lett. **68B**, 497 (1977).
 - [2] R.S. Mackintosh, Eur. Phys. J. A **53**, 66 (2017).
 - [3] R.S. Mackintosh, arXiv:1302.1097v5 (2016).
 - [4] R.S. Mackintosh and N. Keeley, Phys. Rev. **C 76**, 024601 (2007).
 - [5] N. Keeley and R.S. Mackintosh, Phys. Rev. **C 83**, 064608 (2011).
 - [6] R.S. Mackintosh and N. Keeley, Phys. Rev. **C 85**, 064603 (2012).

- [7] R.S. Mackintosh and N. Keeley, Phys. Rev. **C 90**, 064601 (2014).
- [8] N. Keeley and R.S. Mackintosh, Phys. Rev. **C 97**, 014605 (2018).
- [9] H. Feshbach, Ann. Phys. **5**, 357 (1958); Ann. Phys. **19**, 287 (1962).
- [10] G.H. Rawitscher, Nucl. Phys. **A475**, 519 (1987).
- [11] R.S. Mackintosh and A.M. Kobos, Phys. Lett. **B 116**, 95 (1982).
- [12] V. I. Kukulín and R. S. Mackintosh, J. Phys. G: Nucl. Part. Phys. **30** R1 (2004).
- [13] S. G. Cooper and R. S. Mackintosh, Inverse Problems **5**, 707 (1989).
- [14] R.S. Mackintosh, Scholarpedia, 7(11):12032 (2012) doi:10.4249/scholarpedia.12032.
- [15] S. G. Cooper, *Notes for Imago users*, Open University report, (1999) unpublished, available upon request.
- [16] A.M. Kobos and R.S. Mackintosh, J. Phys. G: Nucl. Part. Phys. **5**, 97 (1979).
- [17] A.M. Kobos and R.S. Mackintosh, Acta Physica Polonica, **B 12**, 1029 (1981).
- [18] G.R. Satchler, *Direct Nuclear Reactions* (Clarendon Press, Oxford, 1983).
- [19] C.M. Perey and F.G. Perey, Atomic Data and Nuclear Data Tables **17**, 1 (1976).
- [20] R.S. Mackintosh, Phys. Rev. **C 94**, 034602 (2016).
- [21] A.M. Kobos and R.S. Mackintosh, Ann. Phys. (NY), **123**, 296 (1979).
- [22] M. Ermer, H. Clement, P. Grabmayr, G.J. Wagner, L. Friedrich, and E. Huttel, Phys. Lett. **B188**, 17 (1987).
- [23] M. Ermer, H. Clement, G. Holetzke, W. Kabitzke, G. Graw, R. Hertenberger, H. Kader, F. Merz, and P. Schiemenz, Nucl. Phys. **A533**, 71 (1991).
- [24] A.M. Kobos, G.R. Satchler, and R.S. Mackintosh, Nucl. Phys. **A395**, 248 (1983).
- [25] A.M. Kobos and R.S. Mackintosh, Phys. Rev. **C 26**, 1766 (1982).
- [26] A.J. Koning and J.P. Delaroche. Nucl. Phys. **A713**, 237 (2003).
- [27] R.S. Mackintosh and N. Keeley, Phys. Rev. **C 98**, 024624 (2018).
- [28] R.S. Mackintosh, arXiv:1801.08493 (2018).
- [29] S. Ait-Tahar, R.S. Mackintosh, and M.A. Russell, J. Phys. G: Nucl. Part. Phys. **21**, 577 (1995).